

Article

The Development of a 1-D Integrated Hydro-Mechanical Model Based on Flume Tests to Unravel Different Hydrological Triggering Processes of Debris Flows

Theo W. J. van Asch ^{1,2,*}, Bin Yu ² and Wei Hu ²

¹ Faculty of Geosciences, Utrecht University Princeton 8a, 3584 CB Utrecht, The Netherlands

² State Key Laboratory of Geohazard Prevention and Geoenvironment Protection, Chengdu University of Technology, Chengdu 610059, Sichuan, China; yubin08@cdut.cn (B.Y.); huwei1999@126.com (W.H.)

* Correspondence: t.w.j.vanasch@uu.nl; Tel.: +86-13551168496

Received: 11 June 2018; Accepted: 13 July 2018; Published: 17 July 2018



Abstract: Many studies which try to analyze conditions for debris flow development ignore the type of initiation. Therefore, this paper deals with the following questions: What type of hydro-mechanical triggering mechanisms for debris flows can we distinguish in upstream channels of debris flow prone gullies? Which are the main parameters controlling the type and temporal sequence of these triggering processes, and what is their influence on the meteorological thresholds for debris flow initiation? A series of laboratory experiments were carried out in a flume 8 m long and with a width of 0.3 m to detect the conditions for different types of triggering mechanisms. The flume experiments show a sequence of hydrological processes triggering debris flows, namely erosion and transport by intensive overland flow and by infiltrating water causing failure of channel bed material. On the basis of these experiments, an integrated hydro-mechanical model was developed, which describes Hortonian and saturation overland flow, maximum sediment transport, through flow and failure of bed material. The model was calibrated and validated using process indicator values measured during the experiments in the flume. Virtual model simulations carried out in a schematic hypothetical source area of a catchment show that slope angle and hydraulic conductivity of the bed material determine the type and sequence of these triggering processes. It was also clearly demonstrated that the type of hydrological triggering process and the influencing geometrical and hydro-mechanical parameters may have a great influence on rainfall intensity-duration threshold curves for the start of debris flows.

Keywords: triggering of debris flows; overland flow; infiltration; laboratory experiments; modelling; rain intensity-duration threshold curves

1. Introduction

A debris flow is one of the most dangerous types of mass movement because, depending on the rheology and topography, it can reach a very high speed and large run-out distance. Important study aspects of the initiation process of a debris flow are the mechanism and boundary condition, because they determine the meteorological threshold conditions and further evolution, and will provide clues for future mitigation strategies [1].

One can make different classifications of initiation mechanisms based on different viewpoints [1]. It was among others [2,3], who stressed the importance of the infiltration capacity of the soil as a key factor for either the development of shallow landslides or surficial erosion and transport of material by overland flow, that might create different types of flow like mass movements. Effective overland

flow driven triggering processes are mainly concentrated in channels where high water discharges, and severe erosion and transport lead to high solid concentrations generating debris flows [4–9]. Material is supplied to these debris flows by detachment and transport of the bed material, but also through lateral erosion of the channel bed. The channel can be partly or totally blocked by landslide dams. High runoff discharges eroding these landslide dams can also lead to initiation and rapid growth of debris flows [10–12]. Landslide damming can also be initiated by rapid incision of the channel bed destabilizing the side walls [13]. With infiltrating driven triggering mechanisms, shallow landslides are generated, which may or may not transform into debris flows. This failure mechanism by infiltrating water can occur in channel beds filled with loose material [14] and on planar slopes where shallow landslides can also transform into debris flows [15–18]. The transformation of a failed mass into a debris flow is rather complex and depends on various hydro-mechanical processes related to pore pressure development and supply of abundant overland flow water further mobilizing the failed mass [19–23].

Several authors analyzed partly the role of hydro-mechanical and morphometric factors controlling the type of initiation of debris flows. Berti [24] analyzed the hydrological factors for the generation of debris flows in typical source areas in the Italian Alps by modelling overland flow in the channel bed from a source area as a response to rainfall impulses. Kean [25] proposed an integrated hydro-geotechnical dynamic model to describe sediment transport by overland flow and consequently mass failure transforming into debris flow surges. Hu [26] highlighted the initial soil moisture, and thus infiltration capacity as a controlling factor for the type of initiation; wet soils created mainly surficial runoff, erosion, and incision; bank failure; and damming and debris flow development, while dry soils showed mainly infiltration and landslide failure and debris flow initiation [1]. Zhuang et al. [1] focused more on the slope gradient as a controlling factor for different types of initiation. Their flume studies revealed that at gentler slope gradients around $10^\circ \pm 2^\circ$, incision and bank failure is dominant, creating channel damming and dam failure, inducing debris flows. At intermediate slopes around $15^\circ \pm 3^\circ$, erosion of bed material occurs at high discharges. The high sediment transport capacity with high sediment concentrations is sufficient to create debris flows. At steeper slopes around $21^\circ \pm 4^\circ$, bed failure by infiltrating overland flow water with debris flow formation is the most dominant process.

Meteorological thresholds for the initiation of debris flows are closely related to the process of initiation. In many studies about these meteorological thresholds, no clear distinction was made between the types of triggering [27]. The assessment of these thresholds in relation to various morphometric and geological factors was made in most cases using statistical techniques [28–30].

Until now, only isolated aspects of the hydrological triggering system of debris flows have been studied. There is a need for a comprehensive framework which gives insight in the controlling factors for the evolution of different triggering systems in upstream channels of debris flow gullies. Therefore this paper will try to give answers on the following questions:

1. What type of hydro-mechanical triggering mechanisms for debris flows can we distinguish in upstream channels of debris flow prone gullies?
2. What are the main parameters and in what way are they controlling the type and temporal sequence of these triggering processes?
3. What is the influence of hydro-mechanical parameters and related triggering processes on the meteorological thresholds for debris flow initiation?

In order to answer these questions we have carried out a number of flume tests to detect the conditions for different types of hydro-mechanical triggering mechanisms of debris flows (Section 2). Based on the process information revealed by these experiments we will develop an integrated hydro-mechanical model describing these triggering processes (Section 3). The model will be calibrated and validated using indicator values obtained from the processes measured in the flume (Section 4). Virtual model simulations will be carried out in a schematic hypothetical source area of a catchment to make a framework of the type and sequence of these triggering processes as a function of slope

angle and the hydraulic conductivity of the bed material (Section 5). The model will also be used for sensitivity analyses to study the influence of important geometrical and hydro-mechanical parameters and the related type of initiation process on rainfall intensity-duration threshold curves, for the start of debris flows (Section 6).

2. Flume Tests to Reveal Types of Debris Flow Triggering

2.1. Setup of the Flume Experiments

A flume was designed to see whether we could simulate in a 1D framework the initiation of debris flows by different hydro-mechanical triggering mechanisms. (Figure 1). The flume had a length of 8 m and a width of 0.3 m. The material simulating the channel bed with a thickness of 0.1 m and a width of 0.3 m was positioned at a distance of 4 m from the top of the flume and had a length of 2 m. The material was brought into the flume in layers of about 2 cm and was slightly compacted dry density (see Table 1). There was an outflow at a distance of 2 m from the lower end of the channel bed (Figure 1). The water entered at the upper end of the flume with a controlled discharge, simulating run-on water from an upstream area.

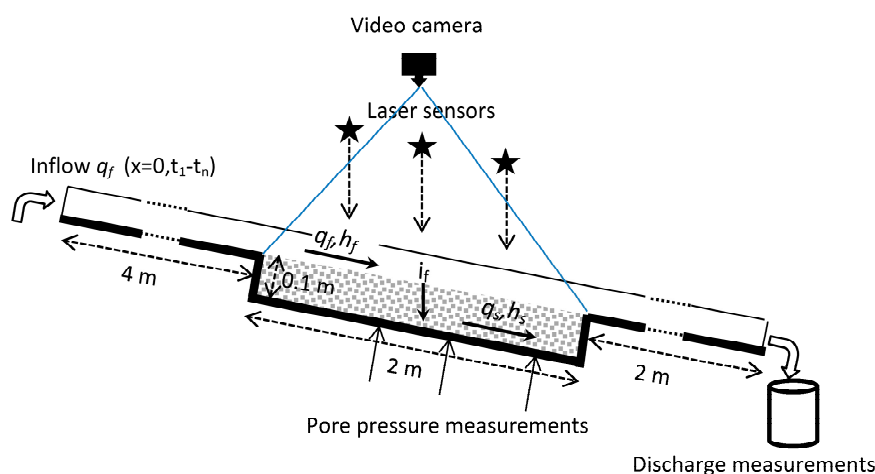


Figure 1. Design of the flume test. For explanation of the parameters see text.

Table 1. Hydro-mechanical characteristics of three types of bed material used in the flume tests. Friction means friction angle of the material in degrees. D30/50 means that 30/50% of the sample had a lower diameter than what is indicated in the column.

Particle Size Class	Friction ϕ (°)	Density $k Nm^{-3}$	SD $k Nm^{-3}$	Hydraulic Conductivity ($m s^{-1}$)	D ₃₀ (mm)	D ₅₀ (mm)	D ₉₀ (mm)
Coarse	34.6	15.4	1.7	4.91E-03	9	11	18
Medium	33.7	16.3	3.0	3.28E-03	4	6	16
Fine	29.2	19.5	1.4	0.54E-03	0.7	1.6	8

Three types of material were used in the experiments with different grain size distributions (Figure 2). The mean density of the bed material was 15.4, 16.3, and 19.4 $k N m^{-3}$ for the coarse, medium, and fine material, respectively with a SD of 1.7, 3.0, and 2.4, respectively. We could vary the slope angle of the flume between 14° and 20°. The initial moisture content of the flume material was more or less dry. The initial moisture content is important for the infiltration capacity, but since we used in the laboratory a large influx of water from above into the coarse bed material, we ignored the effect of the sorptivity (related to the initial moisture content) on the infiltration capacity of the bed material.

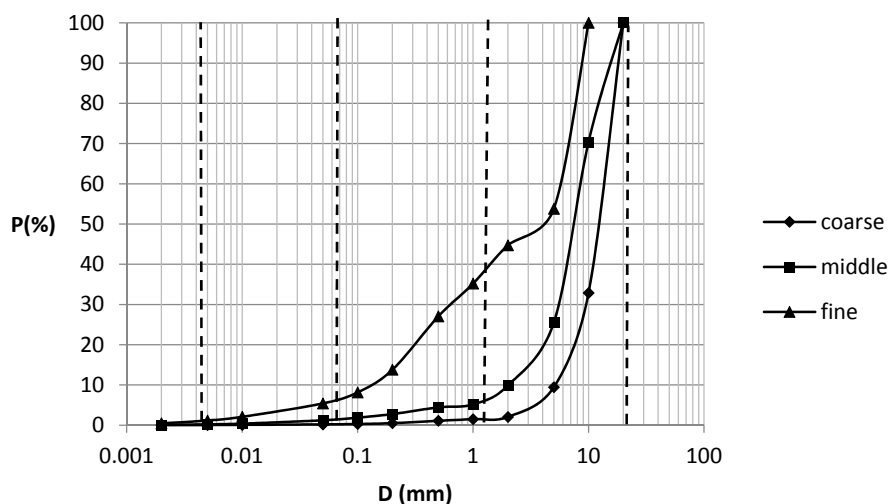


Figure 2. Cumulative grain size distribution of the three bed materials used in the flume tests.

The friction of the three materials was measured with the conventional direct shear apparatus [31]. The hydraulic conductivity of saturated cylindrical soil samples of the three grain sizes was measured with a constant head gradient between the upper and lower end of the sample [32]. Only a limited amount of hydromechanical tests were carried out, which delivered no information about the mean and SD of the friction and hydraulic conductivity values. Table 1 gives further information about the friction, hydraulic conductivity, and gradient of the materials used for the experiments.

Pore pressure was measured at three places (Figure 1) at the bottom of the flume. The pore pressure sensors, type: YP4049, were produced by Yom Technology Company. The measuring range of pore pressure was from -100 k Pa to $+100$ k Pa.

Laser sensors (ZLDS100 ZSY Group; resolution 0.03% FS) at three points with a spacing of 0.5 m (Figure 1) were used to monitor topographical heights, especially with the aim to monitor abrupt changes in relief due to bed failure.

In addition, video recordings were performed (Figure 1) to follow the sequence of processes in the course of the experiments. During the process of overland flow erosion, samples were taken six times for more or less steady state conditions at the outlet of the flume (Figure 1). The discharge of water with sediments was collected in baskets every 5 s. The sediments were sieved, dried, and weighed to determine the solid discharge and the concentration of the fluid. The mean percentage deviation between the individual measurements during an experiment was 32.5% and 19.3% for the water discharge and solid discharge, respectively.

An integrated model (Section 3) for surface and subsurface flow, sediment transport, and bed slope stability was developed to describe the processes in the flume, which was used later to analyze the sequence of different initiation processes at the field scale.

2.2. Observations on Different Types of Hydrological Triggering Mechanisms in Flume Tests

The flume tests were carried out in order to reveal different types of hydrological triggering mechanisms which may create debris flows and to establish indicators related to these triggering processes which were used to calibrate and validate our theoretical model (Section 4). During the flume tests with the three bed materials under different slope angles, observation were carried out by means of video images and laser sensors. Some of the observed process indicators are given in Table 2.

Table 2. Observed time to overland flow and bed failure, overland flow type and failure mode in flume experiments for three types of bed material and for different bed slope angles: (a) saturation overland flow; (b) Hortonian overland flow; (c) slow continuous bed failure; (d) rapid failure; nf: no failure.

Grain size	Slope	Inflow $L s^{-1} m^{-1}$	Time to Run-Off Initiation sec		Time to Bed Failure sec		
Coarse 0.0049	20°	0.18	402		411		
	18°	0.22	103		110		
	16°	0.29	63		72		nf
	15°	0.40	73				
	14°	0.41	59				
Medium 0.0033	20°	0.11	168		168		
	18°	0.13	140		140		
	16°	0.16	54		106		nf
	15°	0.18	27				
	14°	0.19	46				
Fine 0.00054	20°	0.03	30		270		
	18°	0.06	220		613		
	16°	0.09	90		270		d
	15°	0.10	110				
	14°	0.11	102				nf

In slope hydrology, two types of overland flow can be distinguished: saturation overland flow and Hortonian overland flow [32]. These two types could be distinguished during the different flume experiments (Table 2). Saturation overland flow was characterized, after complete saturation of the soil, by a more or less spatially randomly ponding of water at the soil surface, while Hortonian overland flow, which occurs when the rainfall intensity or supply of overland flow water is larger than the infiltration capacity of the soil, showed a more concentrated continuous flow over the length of the flume bed. According to these visual indicators, we could establish a boundary between saturation overland flow and Hortonian overland flow, which in our flume tests was found in the medium grain size materials at a slope gradient of 16° (Table 2). This could be verified with our model simulation (see below Section 5.2). For courser materials (K_s values of $4.91E-0.3$ and $3.28E-0.3 m s^{-1}$) and higher slope angles ($>16^\circ$) the time to saturation overland flow was immediately followed by failure or with a small delay until nine seconds. Also, one could clearly observe that the time to saturation overland flow (and thus failure) decreased with decreasing slope angle (Table 2).

Hortonian overland flow [32] was initiated in most cases on the finer sediments, which is ascribed to the lower infiltration capacity ($K_s = 0.54E-0.3 m s^{-1}$). Bed failure in this case occurred a certain time after the start of Hortonian overland flow with a time lag ranging between 35 and 160 s (Table 2), because in this case, due to the lower percolation rate, it took time to bring the groundwater in the bed material to a critical failure level.

Bed failure initiation is controlled by the bed gradient and the internal friction of the material and occurred in our experiments on slopes of approximately 16 degrees and higher. At lower slope angles, no bed failure occurred (nf in Table 2) and sediment delivery occurred only by overland flow erosion

The medium and course materials show bed failure characterized by slow movements over the total depth combined with fast surficial entrainment of grains by saturated overland flow. Movement of bed material was slow and continuous or sometimes intermittent, showing a surging pattern (Table 2). Instead of the slow and more flow-like movements observed for the medium and coarse sediments, failure of the fine sediments occurred suddenly with a very rapid surge of more or less coherent blocks followed by fluidization (Table 2).

Sediment transport by overland flow on these steep slopes reached volumetric concentrations between 0.46 and 0.64, which is characteristic for debris flows.

We can conclude on the basis of these observations that the flume tests carried out with the three materials revealed three types of processes, which created debris flows in these ranges of slopes gradients, namely debris flow initiation by Hortonian overland flow erosion (RhE-I), saturation

overland flow erosion (RsE-I), and by bed failure (BF-I). The occurrence and sequence of these processes seems to be controlled by slope gradient and hydraulic conductivity of the bed sediment. Figure 3 gives a schematic overview of these process types.

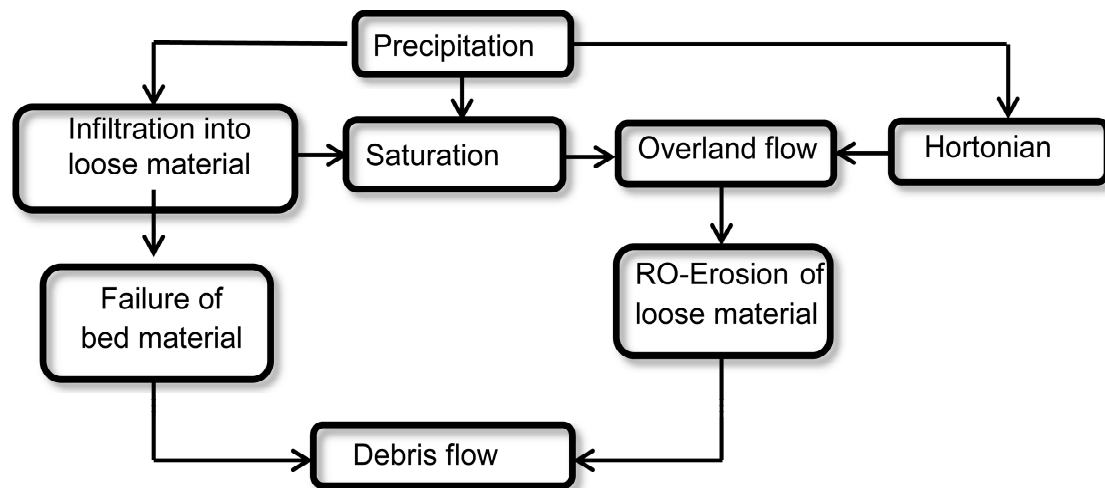


Figure 3. Schematic diagram showing the different initiation processes of debris flows in channels.

3. Integrated Model (1D) for Debris Flow Initiation in Upstream Channels

The flume test observations brought us to the concept of the triggering of debris flows caused by Hortonian and saturation overland flow initiating surficial erosion of bed material. Bed failure and entrainment of material was initiated by infiltration and subsurface flow leading to instability. First, we have to simulate the hydrological component of the triggering mechanisms of debris flows. For that we need the mass balance equation for overland (Equation (1a)) and through flow (Equation (1b)), which is given by:

$$\frac{\partial q_f}{\partial x} + \frac{\partial h_f}{\partial t} = B_1 \tag{1a}$$

$$\frac{\partial q_s}{\partial x} + \frac{\partial h_s}{\partial t} = B_2 \tag{1b}$$

where q_f is overland flow discharge per unit width ($\text{m}^3 \text{m}^{-1} \text{s}^{-1}$); q_s is subsurface discharge per unit width ($\text{m}^3 \text{m}^{-1} \text{s}^{-1}$); h_f is thickness of overland flow (m); h_s (m) is thickness of subsurface flow, ∂x (m) is distance along the slope, ∂t is the time (s), and B_{1-2} are terms (m s^{-1}) describing the inflow or outflow of water from the flow system, which is defined as follows:

$$B_1 = [r - i_f(a) - 0 - i_f(b)] \tag{2a}$$

$$B_2 = i_f \tag{2b}$$

where r (m s^{-1}) describes the external input of rain into and i_f (m s^{-1}) the outflow of water by infiltration out of the overland flow system (Equation (2a)) (see also Figure 1). When there is no supply of rain, like in our flume experiments, $r = 0$. In the case of subsurface flow, i_f in Equation (2b) is considered now as an inflow term of the subsurface flow system. If $h_f/\Delta t$ is larger than the infiltration capacity, K_s (m s^{-1}) of the bed material the latter one is the limiting factor. Therefore the infiltration term i_f of Equation (2) is the minimum (min) value of the infiltration capacity K_s (m s^{-1}) and the current water depth (h_f), which can infiltrate in one time step Δt into the bed material:

$$i_f = \min(K_s, h_f/\Delta t) \tag{3}$$

We introduce here a general momentum equation for the water flow processes [33]:

$$h_f = \alpha_f q_f^{\beta_f} \tag{4a}$$

$$h_s = \alpha_s q_s^{\beta_s} \tag{4b}$$

For turbulent overland flow, the parameters α_f and β_f in Equation (4a) can be defined as follows:

$$\alpha_f = \left(\frac{n}{S_0^{0.5}} \right)^{0.6} \text{ and } \beta_f = 0.6 \tag{5}$$

where n is Manning’s n and S_0 the slope gradient of the bed material.

For subsurface flow we can write according to Darcy’s law:

$$q_s = K_s \sin \theta h_s \rightarrow h_s = \frac{1}{K_s \sin \theta} q_s \tag{6}$$

where q_s is the amount of subsurface flow water per unit width ($\text{m}^3 \text{m}^{-1} \text{s}^{-1}$), θ is slope angle (degrees), and h_s is the height of the flowing water component in the soil matrix (m). By comparing Equation (6) with the general momentum Equation (4b) we can define the parameters α_s and β_s for subsurface flow:

$$\alpha_s = \frac{1}{K_s \sin \theta} \text{ and } \beta_s = 1 \tag{7}$$

A combination of the mass balance Equation (1) with Equation (4) delivers an expression for overland flow or subsurface flow discharge (q_f, q_s) [33]:

$$\frac{\partial q_f}{\partial x} + \alpha_f \beta_f q_f^{(\beta_f s - 1)} \frac{\partial q_f}{\partial t} = B_1 \tag{8a}$$

$$\frac{\partial q_s}{\partial x} + \alpha_s \beta_s q_s^{(\beta_s - 1)} \frac{\partial q_s}{\partial t} = B_2 \tag{8b}$$

The 1D model is implemented in a fixed Eulerian frame where the variation in water flow variables is described at fixed coordinate points at a distance Δx along the slope as a function of time step Δt . A numerical solution for Equation (8) is given by [33]:

$$q_{x+1}^{t+1} = \frac{\frac{\Delta t}{\Delta x} q_x^{t+1} + \alpha \beta q_{x+1}^t \left(\frac{q_{x+1}^t + q_x^{t+1}}{2} \right)^{\beta - 1} + \Delta t \left(\frac{B_{x+1}^{t+1} + B_x^t}{2} \right)}{\frac{\Delta t}{\Delta x} + \alpha \beta \left(\frac{q_{x+1}^t + q_x^{t+1}}{2} \right)^{\beta - 1}} \tag{9}$$

where q_x, α and β should be read as $q_{f,s}, \alpha_{f,s}$ and $\beta_{f,s}$, respectively.

To simulate the initiation of debris flows by mass failure we used the equation for the infinite slope equilibrium model [31], which is the trigger for failure:

$$F = \frac{(\gamma_s z \cos \theta - p) \tan \varphi}{\gamma_s z \sin \theta} \tag{10a}$$

$$p = \gamma_w h_s \cos \theta \tag{10b}$$

where F is the safety factor; failure occurs when $F = 1$; γ_s and γ_w (k N m^{-3}) are the saturated bulk density of the material and water, respectively; φ is friction angle of the material; z and h_s are the thickness of the soil and the height of the groundwater layer, respectively; h_s can be solved with Equation (6) and (9), respectively.

The overall stability of the bed material expressed with the safety factor (F) for the infinite slope model was calculated as an average of the safety factor of the different nodes. The inflow of water into the flume is coming from upstream, and therefore the pore pressure gradient is decreasing downstream. This means that the safety factor is always increasing downstream, and therefore the average approach of the safety factor over the length of the sample in the flume seems a reasonable approximation of the overall safety factor.

For estimating the transport capacity on steep slopes Rickenmann [34,35] proposed a bedload transport equation based on a shear stress approach, where discharge, bed slope gradient, and material grading are used as parameters to characterize flow hydraulics.

For steeper slopes, in the range of $0.03 < S < 0.2$ (1.7° – 11.3°), Rickenmann [34] performed a regression analysis with the steep flume data on bed load transport obtained at ETH Zurich that resulted in the equation:

$$q_{solid} = \frac{12.6}{(d_s - 1)^{1.6}} \left(\frac{D_{90}}{D_{30}} \right)^{0.2} (q_f - q_c) S^2 \quad (11)$$

where D_{90} and D_{30} are grain sizes at which 90% and 30%, respectively, by weight of the material are finer; d_s is the mass density of the solids, S is the slope gradient, and q_c is the critical flow discharge for bedload entrainment. The experimental slopes were in the range of $0.03 > S > 0.20$ (1.7° – 11.3°), and the D_{90} of the material ranged between 0.9 and 2 cm and D_{30} between 0.06 and 1 cm with inflow rates of 10 – 30 L s^{-1} . In the section below, we will calibrate Equation (11) for the steeper slopes in our flumes.

The integrated model developed in this section is able to describe the different types of hydro-mechanical triggering mechanisms for debris flows. It delivers us the physical parameters, which controls these processes, which will be applied in our virtual simulations in Sections 5 and 6.

In the next section, we will calibrate our model on some process indicator values obtained from our flume tests.

4. Calibration and Validation of the Theoretical Model on the Basis of Flume Test Results

We will use here a number of process indicator values measured during the flume experiments to calibrate and validate the outcomes of our theoretical model. These are saturation or Hortonian overland flow, time to overland flow, maximum pore pressure, time to bed failure, and solid concentration by overland flow erosion. Hortonian overland flow and the time to Hortonian overland flow in the model is declared when surface water h_f reaches the lower end of the bed material, while the bed material is still not saturated ($h_s < Z_s$). Saturation overland flow and the time towards it is declared when $h_s = Z_s$ over the entire bed. Pore pressure is calculated each time step according to Equation (10b). The discharge of $h_f + h_s$ is reported each time step at the end of the flume. Bed failure is declared as mentioned earlier when the average safety factor F over the bed length reaches the value of 1.

For the flume simulations, the distance between the nodes (Δx) was 0.1 m and the time interval (Δt) was 0.2 s.

Figure 4 shows the relation between observed and calculated time to overland flow for the different flume tests. There is a moderate 1:1 correlation between observed and predicted time to overland flow for the medium and coarse sediments and for the fine sediments, showing Hortonian overland flow there is no correlation at all. The deviations in observed and predicted time to overland flow can be ascribed to the variation in density of the bed material in combination with a poor estimate of the K_s value based on a limited amount of measurements, which was used as input for the modelling (see Section 2.1). However the model was able to predict the type of overland flow according to what was observed during the flume tests (see Table 2).

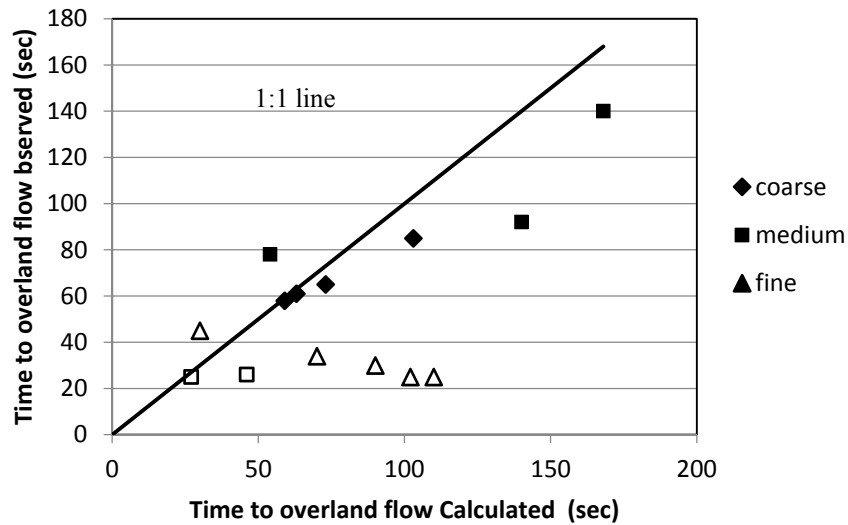


Figure 4. Observed and calculated time to saturation overland flow (black symbols) and Hortonian overland flow (open symbols).

Despite the malfunctioning of some pore pressure sensors we were able to make a 1:1 comparison between the average maximum measured pore pressure for the three sensors (Figure 1) and the average calculated maximum pore pressure (Figure 5).

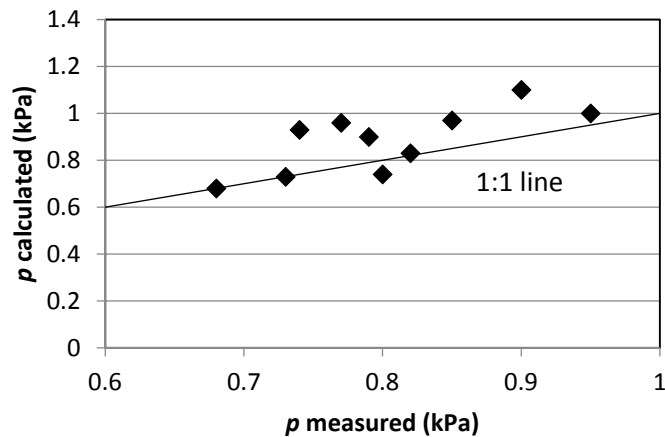


Figure 5. Maximum pore pressure measured during flume tests in relation to calculated pore pressures.

The Figure shows that in many cases there is a slight overestimation of the calculated pore pressure. Time series of measured pore pressure of the three sensors compared to modelled temporal pore pressure development showed that in most cases the onset towards maximum pore pressure for the three sensors was more irregular compared to the calculated development of the pore pressures (Figure 6). This can be ascribed to the variation in density, which occurred during the compaction of the sediment layers or (and) the imperfect response of the sensors.

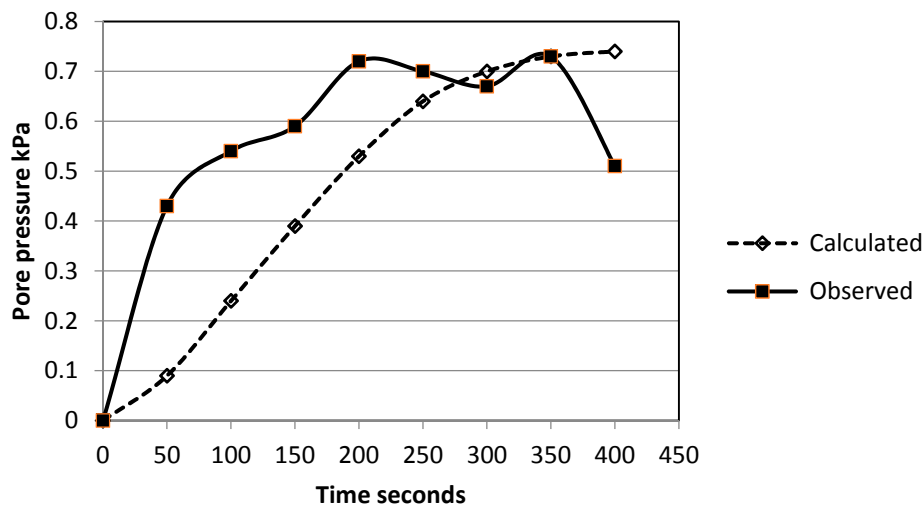


Figure 6. Example of the rise in pore pressure (measured/calculated) due to infiltration of run-on water in the bed material (test: medium grain size/20°).

In relation to pore pressure development we compared the time to failure for the different test runs on the different materials. Since the time towards average maximum calculated and measured pore pressure coincided more or less, one would expect also corresponding calculated and measured failure times. Table 2 and Figure 7 show that the match between observed and calculated failure time is reasonable except for two outliers (coarse-20°; fine-18°). Figure 7 shows further that the calculated time to failure seems to be underestimated for the coarse material and, although not so clear, overestimated for practically all the tests on the medium and fine materials. This suggests that the percolation rate is lower, and hence the observed time to failure is higher for the coarser bed materials and higher for finer bed materials. The average volumetric concentrations of the runoff water are 0.62, 0.65, and 0.70 for the coarse, medium, and fine bed materials, respectively. However, we would expect lower percolation rates (and therefore higher times to failure) in finer bed materials with higher concentrations of runoff water and more fine material and vice versa: higher percolation rates on the coarser bed materials with lower runoff concentrations. We must conclude that the effect of concentration and gradient of the sediment in the water is not visible in our observed time to failure. Therefore, the deviations between calculated and observed values must be ascribed to the heterogeneity of the material, incorrect estimate of the friction values, and K_s values and bulk density of the percolating water, and incorrect assessment of the overall safety factor.

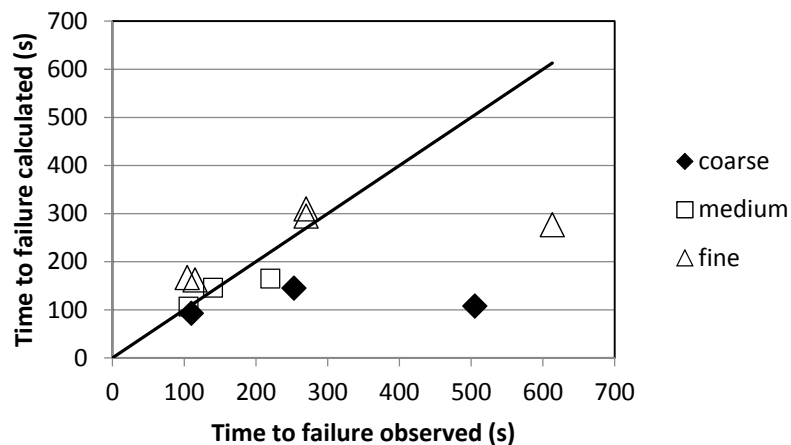


Figure 7. Observed and calculated time of failure of bed material during the flume tests.

We calibrated also the parameters of the Rickenmann [35] equation, (Equation (11)) on our flume tests, which were carried out on slopes ranging between $0.25 > S > 0.36$ (14° – 20°), with grain sizes for $0.9 > d_{90} > 2$ and $0.05 > d_{30} > 1$ cm, and with flow rates $0.5 > q_f > 15 \text{ L s}^{-1} \text{ m}^{-1}$. Figure 8 shows the best linear fit between q_{solid}/q_f and $(d_{90}/d_{30})^{0.2} S^2$, which delivered the following modified equation for slopes between 14° and 20° :

$$q_{solid} = 7.28 \left(\frac{D_{90}}{D_{30}} \right)^{0.2} q_f S^2 \tag{12a}$$

which gives for $d_s = 2.6$:

$$q_{solid} = \frac{15.44}{(d_s - 1)^{1.6}} \left(\frac{D_{90}}{D_{30}} \right)^{0.2} q_f S^2 \tag{12b}$$

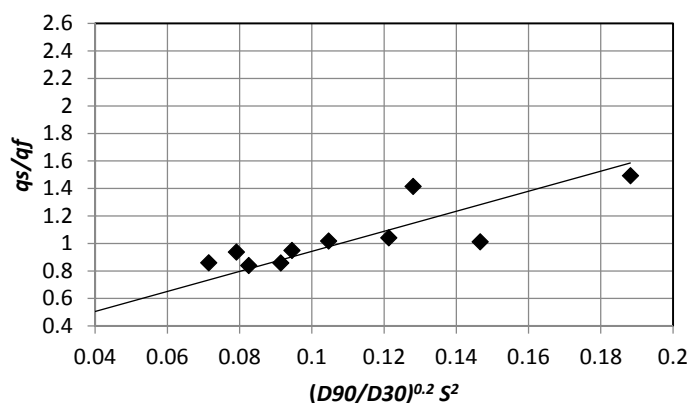


Figure 8. Calibration of Rickenmann’s bedload equation for steeper slopes in our flume tests between 14 and 20 degrees.

The calibration revealed that q_c in Equation (11) becomes zero or practically zero in Equation (12). At slopes larger than 15° the down slope component of the grain weight may reduce the critical shear stress τ_c which in our case obviously reduced to nearly zero.

We may conclude that the model is able to predict in a reasonable way essential process indicators for different hydrological triggering processes of debris flows in upstream channels. In the next section, we will apply the model on the field scale to predict hydro-mechanical triggering patterns for debris flows as a function of the hydrological conductivity of the bed material and the channel slope gradient.

5. Hydro-Mechanical Triggering Patterns for Debris Flows in Relation to Hydrologic Conductivity of Bed Materials and Channel Gradient

5.1. The Design of a Schematic Source Area at the Field Scale

First, we will design a virtual landscape of a potential debris flow source area where our model can be applied to analyze the influence of terrain parameters on the type of triggering mechanisms (Section 5.2) and the meteorological thresholds of debris flows (Section 6).

Figure 9 shows this virtual source area, which is linked to an upstream channel filled with bed material receiving surface water from the surrounding slopes to initiate a potential debris flow. This geomorphological setting resembles more or less the source areas described among others by Coe [7] and Berti [24]. The upstream area of our hypothetical catchment has a radius R . The channel is further surrounded by lateral slopes with a length L . The length of the channel bed is Lx , the width W , and the slope angle is θ . The hydraulic conductivity of the bed material is Ks , the porosity Por and, the friction angle φ (Figure 9).

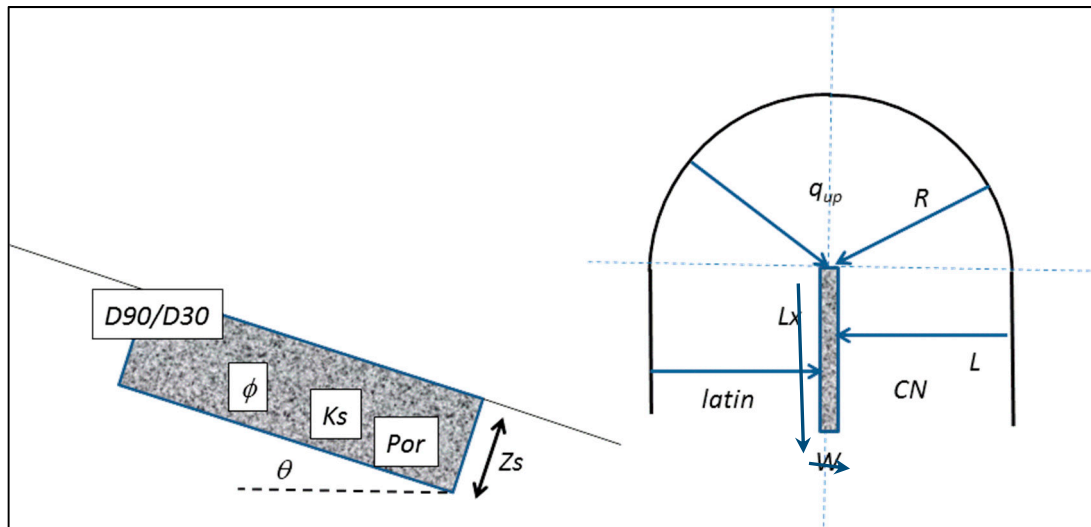


Figure 9. Morphometric and hydro-mechanical parameters, which were used for model simulations of debris flow initiation. For an explanation see Table 3 and text. D90/D30: 90% and 30% lower than grain size D90 and D30, respectively. ϕ : Friction angle; K_s : Hydraulic conductivity; Por : Porosity; Z_s : Depth of material; θ : Slope angle; q_{up} : Water that flows into the upper end of the channel bed; R : Radius of source area above the channel; L_x and W : Length and width of the channel bed; L : Length of lateral contributing slope; $latin$: Lateral inflow of water to the channel; CN : Curve number value for the soil hydrological and land use characteristics of the contributing slopes.

The sink term B in (1) and (8) is now adapted to the field scene and given by:

$$B = 2latin + r - i_f \tag{13}$$

where $latin$ ($m\ s^{-1}$) is the lateral inflow of overland flow water from the slopes along the channel (Figure 9), r direct rain intensity input to the channel bed, and i_f infiltration rate into the bed (see Equation (3)). The lateral inflow is calculated for these sensitivity analyses in a simple way, assuming steady state conditions in the mass balance equation for overland flow:

$$latin = \frac{r_{cn}L}{W} \tag{14}$$

r_{cn} ($m\ s^{-1}$) is calculated using the curve number method [36], L is the length of the lateral slope, and W the width of the channel (see Figure 9). In our simulations we selected overland flow supplying slopes with soils with moderate to slow infiltration rates and a poor condition grass cover, which corresponds to a curve number (CN) of about 80. The CN number, reflecting the hydrological soil characteristics, land use, and antecedent soil moisture conditions that we can expect in high mountainous areas, was chosen arbitrarily and was kept constant in our simulations. The overland flow water that flows into the upper end of the channel bed is given by q_{up} ($m^2\ s^{-1}$) (Figure 9).

$$q_{up} = \frac{r_{cn}0.5\pi R^2 \cos \theta}{W} \tag{15}$$

5.2. The Influence of the Hydraulic Conductivity (K_s) and Slope (θ) of the Channel Bed on the Type and Sequence of Hydrologic Triggering Processes for Debris Flows

In the flume we could observe the effect of slope angle and hydraulic conductivity on the type and sequence of triggering processes, which may lead to the initiation of debris flows. In this section we will investigate with our theoretical model the effect of these two factors at the catchment scale.

The values of the other factors used in our model simulations are shown in bold as default parametric values (Z_s , φ , W , L_x , Por , R , L , n , bed) in Table 3 (see also Figure 9).

Table 3. Default values (bold italic) and maximum and minimum values of input parameters for overland flow erosion (RE-I) and bed failure (BF-I) triggering debris flows. K_s : Saturated hydraulic conductivity; Z_s : Thickness of bed material; φ friction angle of material; θ : Slope angle of channel bed; W and L_x : width and length of channel bed respectively; Por : Available volumetric pore space; R : Radius of source area; L : Length of lateral slopes; n : Manning's n of bed material.

K_s for RE-I	0.001– 0.0025 –0.005 m s ^{−1}	L_x	50– 100 –200 m
K_s for BF-I	0.001– 0.01 –0.1 m s ^{−1}	Por	0.4– 0.3 –0.2
Z_s	2– 4 –6m	R	250– 350 –450 m
φ	28– 32 –36	L	250– 350 –450 m
θ	16°– 20 –28°	n bed	0.08
W	2– 4 –6-m		

Table 4 gives the range in K_s values (first row) and bed slope angles (first column), which were used in our simulations to study the effect of these parameters on the hydro-mechanical process development at the catchment scale. For these simulations, two rain scenarios were used with an intensity of 80 mm (Table 4a) and 40 mm per hour (Table 4b), respectively. The tables show domains with different shades of gray with various combinations of hydro-mechanical triggering processes. In the white sections, no debris flow initiation is expected to develop in the source area because of a too low sediment concentration of the overland flow. Table 4a shows that in the domain $\theta = 28^\circ$ – 20° and $K_s = 0.001$ – 0.005 m s^{−1}, the debris flow is initiated in the first stage by Hortonian overland flow erosion (R_h E-I). The overland flow discharge reaches a steady state after a certain relatively short time. During the steady state, groundwater will rise by infiltration of run-on water until failure of the bed material, which happens between 1.7 and 11.2 minutes depending on the slope θ and K_s . In Table 4a, we see a dramatic drop in discharge between slopes with $K_s = 0.001$ and 0.005. The last K_s value reaches a significant boundary which determines whether or not a debris flow can be initiated by Hortonian overland flow transport.

It is confirmed by Table 4b, with a lower rain input (40 mm) where at $K_s \geq 0.005$, no initiation by Hortonian overland flow is possible anymore.

Going back to Table 4a, in the domain $\theta = 16^\circ$ – 12° and $K_s = 0.001$ – 0.005 m s^{−1} slope failure does not occur. The debris flow is initiated by overland flow; first by Hortonian overland flow and later when the groundwater has reached the surface by saturation overland flow. Discharge is relatively low when there is Hortonian overland flow, while obviously discharge dramatically increases at saturation overland flow. However, due to the lower slope angles, the volumetric sediment concentration is low (0.21 at 16° and 0.13 at 12°) (Table 4a, last column), which means the flow changes from a hyperconcentrated flow into a water flood with conventional suspended load and bed load.

At higher conductivities in the domain $K_s = 0.01$ – 0.1 m s^{−1} and $\theta = 28^\circ$ – 20° , bed failure seems the most dominant process (Table 4a). Due to the larger K_s values, infiltration into the bed is more important than overland flow discharge. The bed material turns out to be partly saturated in the upper part due to the larger upstream inflow, creating partly saturation overland flow and Hortonian overland flow. However, within one minute after the runoff discharge reached the lower end of the bed, failure of the bed material occurred already. Therefore, the contribution of overland flow to the transport of debris by overland flow can be ignored.

In the domain $K_s = 0.01$ – 0.1 m s^{−1} and lower slope gradients ($\theta = 16^\circ$ – 12°), there is no slope failure but only saturation overland flow, (Table 4a) with low sediment concentrations in most cases not enough to call it a debris flow.

Table 4b shows the simulation results with an intensity of 40 mm per hour. The domains with a specific combination of hydro-mechanical triggers still exist. There is only a shift of the boundary for the K_s -values with no Hortonian overland flow (>0.005 m/s) to the left. The Table 4a,b show a

decrease in overland flow discharge and increase in time to bed failure with a decreasing slope angle. Around 16 degrees the channel bed is stable but still steep enough to have transport capacities with concentrations in the domain of a hyper concentrated flow. These are induced by Hortonian and Saturation overland flow at lower K_s values and only Saturation overland flow at higher K_s values. At lower slope angles (see slopes around 12 degrees) sediment concentrations are too low to call it a debris flow. Table 5 gives a summary of the type and sequence of initiation processes related to different K_s and slope angle values.

Table 4. Time sequence of different initiation processes R_h E-I and R_s E-I, (erosion by Hortonian and saturation overland flow respectively) and BF-I (bed failure) in relation with hydraulic conductivity (K_s) and slope angle of bed material. Further are given the discharge (discharg) and solid concentration (concent) during R_h E-I and R_s E-I. Tables 4a and 4b: simulated rain intensities of 80 mm and 40 mm, respectively.

a										
80 mm	K_s	0.001 m s ⁻¹		0.005 m s ⁻¹		0.01 m s ⁻¹		0.1 m s ⁻¹		
Slope Degrees	Initiat Proc.	Time min.	Dischar L s m ⁻¹	Time min.	Dischar L s m ⁻¹	Time min.	Dischar L s m ⁻¹	Time min.	Dischar L s m ⁻¹	Vol Concent L L ⁻¹
28	R_h E-I	1.0	912	1.3	139					0.47
	BF-I	5.4		1.7		2.4		3.0		
24	R_h E-I	1.0	783	1.3	119					0.39
	BF-I	8.4		2.3		2.8		3.1		
20	R_h E-I	1.1	683	1.4	104					0.30
	BF-I	11.2		2.9		3.1		3.1		
16	R_h E-I	1.1	606	1.5	92					0.21
	R_s E-I	14.2	732	3.7	733	3.7	732	3.6	705	
12	R_h E-I	1.2	550	1.5	83					0.13
	R_s E-I	14.8	666	3.9	665	3.8	664	3.6	646	

b										
40 mm	K_s	0.001 m s ⁻¹		0.005 m s ⁻¹		0.01 m s ⁻¹		0.1 m s ⁻¹		
Slope Degrees	Initiat Proc.	Time min.	Dischar L s m ⁻¹	Time min.	Dischar L s m ⁻¹	Time min.	Dischar L s m ⁻¹	Time min.	Dischar L s m ⁻¹	Vol Concent L L ⁻¹
28	R_h E-I	1.5	162							0.47
	BF-I	5.8		7.2		7.9		8.0		
24	R_h E-I	1.6	139							0.39
	BF-I	8.8		7.8		8.2		8.3		
20	R_h E-I	1.7	121							0.30
	BF-I	11.7		8.5		8.5		8.4		
16	R_h E-I	1.8	108							0.21
	R_s E-I	14.8	234	9.5	235	9.4	233	9.3	208	
12	R_h E-I	1.9	98							0.13
	R_s E-I	15.0	214	9.6	213	9.5	212	9.2	170	

Table 5. Sequence of different initiation processes for debris (hyperconcentrated) flows in relation to the hydraulic conductivity and slope of the channel bed material. Simulated rain intensity is 40 mm.

40 mm	K_s Values	0.001 m s ⁻¹	0.005 m s ⁻¹	0.01 m s ⁻¹	0.05 m s ⁻¹	0.1 m s ⁻¹
Gradient	Flow type	Initiation process		Initiation process		
28°	Debris flow	t1: Hortonian overland flow		t1: Bed failure		
24°		t2: Bed failure				
20°						
16°	Hyper -concentratedflow	t1: Hortonian overland flow		t1: Saturation overland flow		
		t2: Saturation overland flow				
12°	No debris flow	t1: Hortonian overland flow		t1: Saturation overland flow		
		t2: Saturation overland flow				

We designed a framework, which gives insight in what kind of debris flow initiation can be expected for a given slope gradient and hydraulic conductivity of the material. In the next section, we will give an impression how different hydro-mechanical parameters of triggering processes can influence meteorological thresholds for debris flows.

6. Sensitivity Analyses for Parameters Influencing the Rain Intensity-Duration (I-D) Threshold Curves for Different Initiation Processes of Debris Flows

In the foregoing, we revealed the influence of K_s and bed slope gradient on the sequence of processes mechanisms involved in the initiation of debris flows. We want to investigate here the effect of the other parameters (including K_s and slope gradient) on rainfall thresholds in terms of intensity duration (I-D) curves for the triggering of debris flows by two main process mechanism: initiation by Hortonian overland flow (R_hE-I) and bed failure (BF-I). As we have seen in Tables 4 and 5, debris flow initiation by saturation overland flow (R_sE-I) can only take place around 16 degrees. At lower slope angles, sediment concentrations are too low to call it a debris flow (Table 4). At higher slope angles, we have bed failure before saturation overland flow can take place.

Figure 10 shows the effect of different parameters on the I-D curves for debris flows initiated by Hortonian overland flow. The intensity and duration value of a rain event which creates overland flow that just reaches the end of the channel bed with a sediment concentration of >0.2 , is defined by us as a threshold rain event for debris flow initiation. The intensity and duration values for a variety of different critical rain events were plotted in a graph with on the Y-axis the intensity and on X-axis the duration. In this way, an intensity duration (ID) curve can be constructed. Table 3 gives an overview of the range of the different parameters and the default values (in bold italic), which were used in the simulation and which give a realistic representation of geometric and geotechnical parameters for source area conditions. The threshold curves for debris flow initiation by Hortonian overland flow are shown in Figure 10. In this figure, the threshold curves, which are constructed using the default values given in Table 3, are depicted with open rectangular markers. They are equal in all the sub-figures. This enables one to compare for the different parameters the difference between the ultimate curves and the default curve. For each selected parametric value there is an ultimate minimum rain intensity below which not enough overland flow, and thus a debris flow can be initiated, irrespective the duration (D) of the rain event (see horizontal dotted lines).

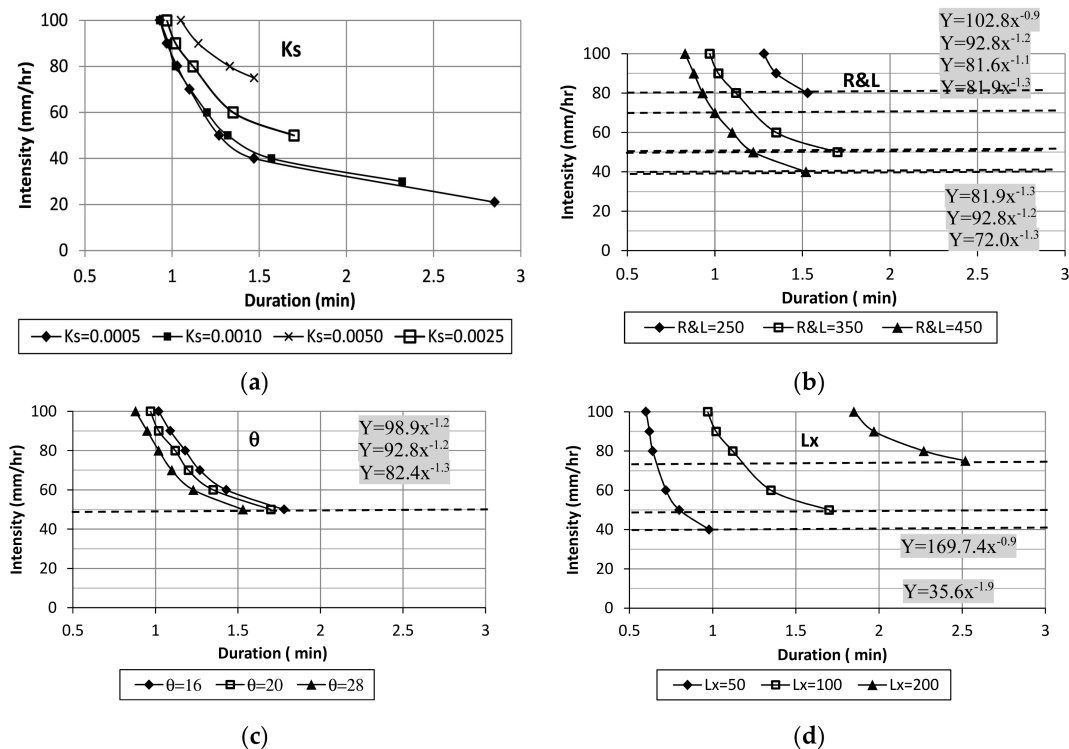


Figure 10. Cont.

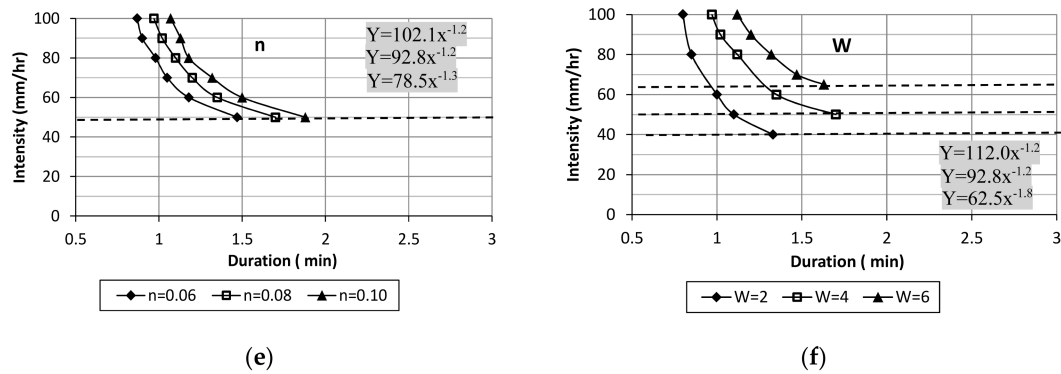


Figure 10. I-D curves for debris flow initiation by Hortonian overland flow in relation to different geometrical and hydrological parameters. The regression formula belong to the curves from top to bottom. For the definition of parameters see Table 3.

The simulations show that at intensities below this critical dotted line the overland flow water never reach the lower end of the bed due to a too high infiltration rate on its pathway compared to the supplied amount of water (direct rain input and surrounding overland flow), and finally bed failure may be the primary triggering process.

The most obvious selected parameter for overland flow initiation is the hydraulic conductivity K_s . Other parameters are related to geometry of the source area (see Figure 6) like length of the lateral slopes along the channel (L), radius of the upstream area of the channel (R), Length (L_x) and width (W) of the channel bed, channel bed gradient (θ), and further Manning's n of the bed material.

We saw in the forgoing that Hortonian overland flow plays a dominant role for K_s values $<0.005 \text{ m s}^{-1}$. Figure 10a shows the influence of the K_s value on the I-D threshold curves for runoff erosion initiation (R_hE-I). The range of K_s values was chosen between 0.0005 and 0.005 m s^{-1} . The figure shows that for K_s values lower than 0.001 m s^{-1} there is nearly no effect of K_s on the position of the I-D curve, but there is a difference in the minimum intensity values (dotted lines) below which no debris flow can occur. A slight difference can be observed for lower intensities ($<60 \text{ mm h}^{-1}$). Higher K_s values ($>0.001 \text{ m s}^{-1}$) have a larger influence on the I-D curves. (Figure 10a).

The simulations show that the scale of the source area and lateral slopes ($R&L$), the length of the river bed (L_x), and the width of the bed (W) have the largest effect on the position of the threshold curve for the initiation of debris flow by Hortonian overland flow (Figure 10b,d,f, respectively). The threshold curves are less sensible for the effect of the slope gradient θ and Manning's n of the bed material (Figure 10c,e respectively).

Figure 11 shows the influence of the different geotechnical and geometrical factors on the threshold values for the triggering of debris flows by bed failure. The range in K_s values for which bed failure (BF-I) is the dominant process were chosen between 0.001 and 0.1 m s^{-1} with a default value of 0.01 m s^{-1} . The effect of the selected range in geometric values $R&L$, L_x , W , θ , and Z_s (Figure 11b,d,f-h, respectively) seems to be more or less the same. Less effect has the porosity (Por) of the bed material and the ϕ values (Figure 11c,e, respectively). No effect had the hydraulic conductivity K_s (Figure 11a), which is related to the simplicity of the model describing instantaneous downward percolation for these high permeable bed materials. Interesting was to see that at lower K_s values (around 0.001 m s^{-1}) and higher rain intensities, the rate of groundwater storage, and therefore the critical duration for failure, was nearly the same (Figure 11a).

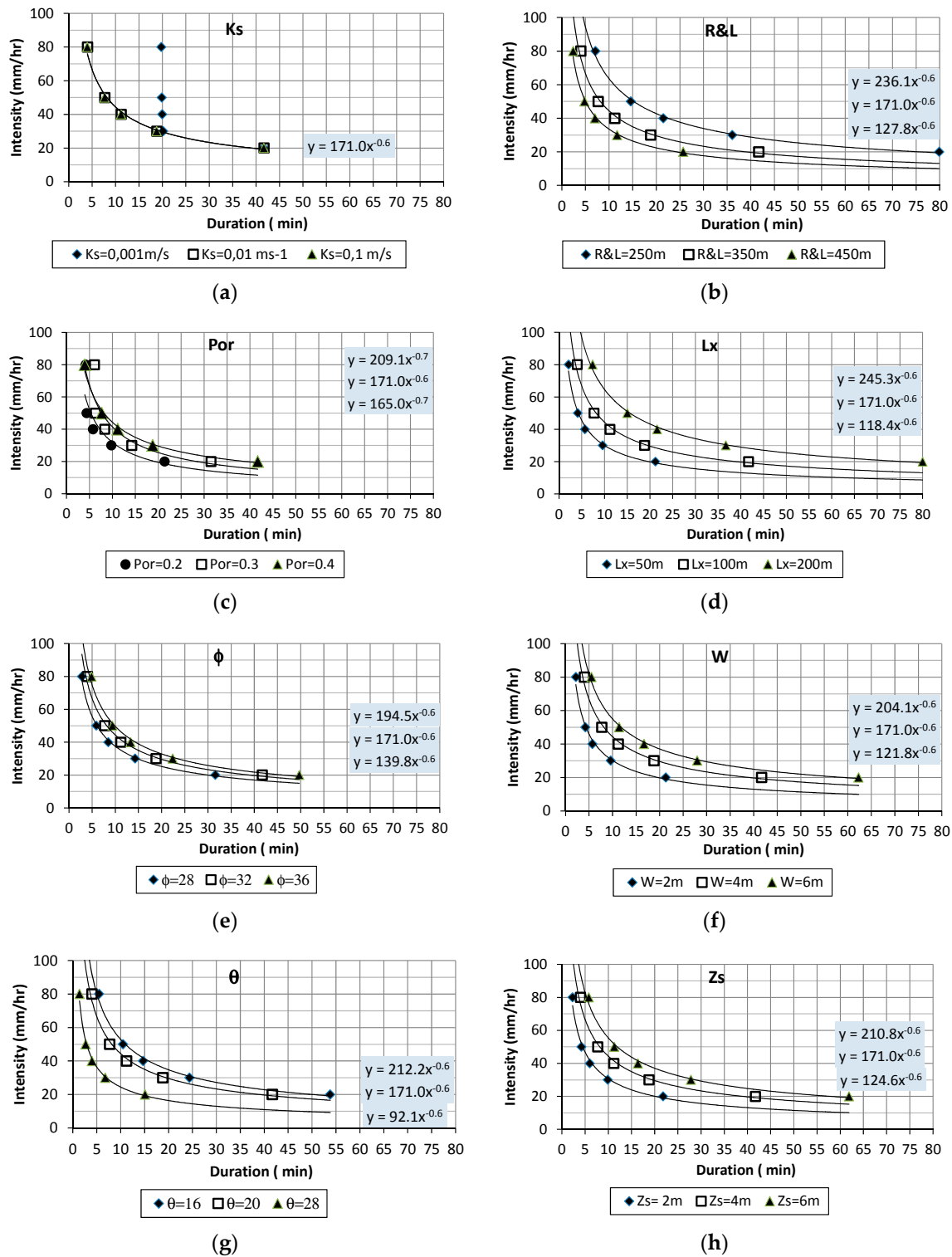


Figure 11. I-D curves for debris flow initiation by bed failure in relation to different geometrical and hydro-mechanical parameters. The regression formula belong to the curves from top to bottom. For the definition of parameters see Table 3.

The I-D curves obtained by our simulations suggest that the duration range was strongly influenced by the type of initiation. Debris flows initiated by Hortonian overland flow seems to be initiated within several minutes while debris flow initiated by bed failure within one to two hours.

I-D curves found in the literature give threshold curves with a larger duration range of one to several hours. The relative quick response to debris flow initiation can be explained by the large effect we give in our simulations to the contributing slopes with sparse vegetation and low infiltration rates, which in other areas may be minor due to higher infiltration rates of denser vegetation and lower overland flow rates. The use of the curve number method also explains the quick response to initiation, because it does not take into account the effect of the initial moisture content which for dry soils gives larger infiltration rates and time to ponding in the first period of a rain event. It also does not simulate the travel time towards the channel. The relative quick response for channel bed failure initiation was also found by Berti [24] dealing with nearly impermeable rock slopes in the source area.

Figure 12 compares two extreme I-D curves [37,38], and one in between the two [39] obtained worldwide with the two extreme curves produced in our simulation. The minimum curve in our simulation was related to the maximum channel slope (28°), and the maximum threshold curve was related to the largest length (Lx) of the channel bed. Figure 12 shows that a simple variation of parameters for the initiation of debris flows in channel beds of source areas, which gives already a significant range in variation compared to the range in threshold values for debris flows worldwide. The figure shows that, for reasons given above, our simulated curves are positioned in the lower part of the domain covered by all the curves obtained from different parts of the world.

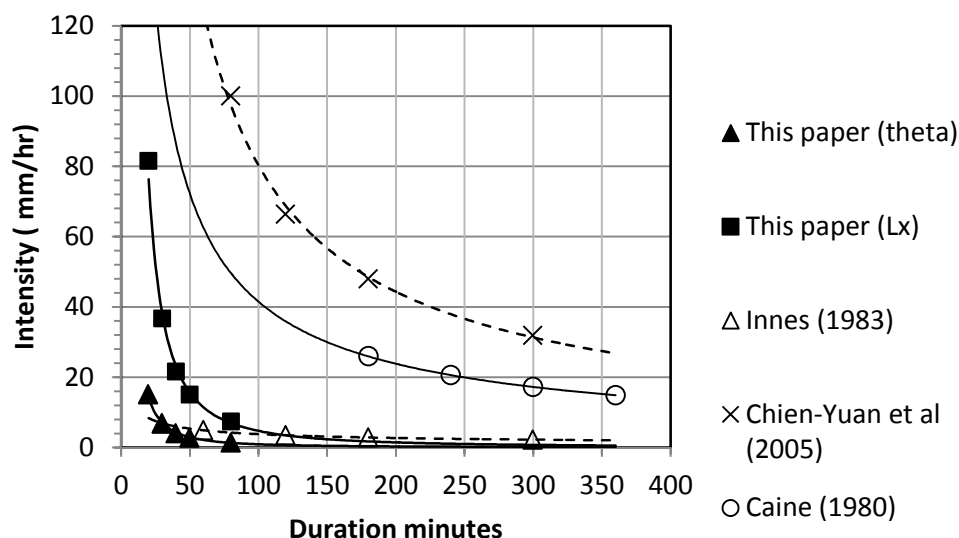


Figure 12. Ultimate variation in I-D curves as a result of our sensitivity analyses compared to the maximum difference in I-D curves found worldwide.

We have shown in this section that the I-D curves for debris flows triggered by overland flow and bed failure are especially sensitive to the morphometric parameters of the source area and less sensitive to the hydro-mechanical parameters. The I-D curves for debris flows, triggered by the overland flow process are more sensitive to these parameters than the I-D curves related to the bed failure triggering process (compare Figures 10 and 11). The sensitivity of these curves for these process parameters cover a range, which is quite significant compared with the ultimate range of I-D curves found worldwide.

7. Discussion

This paper unraveled the effect of different hydro-mechanical processes on the initiation of debris flows. It is focused on the initiation in channels and it gives a detailed insight in the influence of different hydro-mechanical process mechanisms in the source area on the type of debris flow initiation. It shows how the hydrologic conductivity (Ks) and slope gradient (θ) determine the sequence of various process mechanisms.

Our simulations suggest that the type of initiation and related factors have also a clear influence on the values of the I-D curve as shown in Figures 10 and 11. These I-D curves, determined by our two simulated process mechanisms, Hortonian overland flow and bed failure show a relative quick response of debris flow initiation compared to what is generally provided by the literature. Our calculations were focused on the initiation of debris flows in the source area in channel beds surrounded by slopes with scarce vegetation and rather impermeable soils. A quick response (within one hour) was also observed by Berti [24] where, as in our simulations, debris flows were initiated in the source area by the dominant effect of run-on water to the channel delivered by a bare, impermeable catchment upstream.

The assessment of rainfall threshold values for debris flow initiation are based in most cases on statistical empirical approaches using large data sets without detailed knowledge of the different triggering processes and its influencing factors [2,29]. Our quantitative approach to analyze the threshold conditions for debris flow initiation gives a more detailed insight in the effect of different parameters than the indicative parameters used in statistical techniques. Apart from the fact that no distinction is made in the mechanism of initiation, important morphometric characteristics, like channel width, slope, length, and thickness of bed material are ignored in most cases. As a consequence, the prediction of the probability debris flow initiation on the basis of rainfall for individual catchments can be very inaccurate. Further investigations must reveal the accuracy of both approaches to predict the initiation of debris flows.

The CN value, which we used in the simulation of overland flow on the contributing slopes, reflects in a lumped way the dynamic soil and land use characteristics. Especially the amount of storage of water before the time to ponding, and thus the estimate of the total overland flow production of a rain event can be rather inaccurate, especially for rain events with shorter durations. The use of a more detailed infiltration model incorporating the effect of the initial moisture content will give better predictions. However, in this paper we did not unravel in detail the effect of these soil and land use characteristics on threshold conditions for debris flow initiation, but used a constant CN value as input for the run-on simulation to the channel bed. Initial moisture conditions in the channel bed, which will affect the permeability and hence the boundary conditions for the initiation of overland flow were not considered either in this paper. The effect of the initial moisture content of the bed material is minor due to the large amounts of influx of water and the relative coarse material in the channel bed.

In this paper we mentioned the transport capacity of overland flow as a limiting factor for the initiation of debris flows. On slopes ($<\pm 16^\circ$) sediment concentrations are too low (<0.2) to call it a debris or hyper-concentrated flow. For these lower channel gradients we did not consider the effect of the delivery of extra material by side wall collapses and failure of landslide dams [1,13,40], which may lead downstream to a rapid loading of the fluid and an instantaneous transformation into a debris flow

The initiation of debris flows by bed failure is also more complex since it depends on certain boundary conditions related to pore pressure development at failure and a large amount of runoff water, which must be supplied during failure to keep the material moving [20,22,23,41,42].

It is interesting to analyze the potential in development further downstream of debris flows triggered by bed failure (BF-I) with high solid concentrations. On steeper slopes failure of the bed material occurs under lower groundwater heights (h_s), and therefore after failure much additional overland flow water is needed to maintain the movement further down slope. Important is also the mechanism of erosion and erosive power of both types of debris flows further downstream in order to grow to a mature debris flow [6,43–47].

8. Conclusions

We could distinguish in our flume tests three types of hydro-mechanical processes which may trigger debris flows in channel beds of first order source areas. These are erosion and transport by intensive Horton overland flow (RO_h-I), saturation overland flow (RO_s-I), and by infiltrating water causing failure of channel bed material (BF-I). On the basis of these flume tests, an integrated

hydro-mechanical model was developed, which was calibrated and validated with a number of process indicators measured during the flume tests. We were able to assess by means of this model the influence of important parameters on the mode of debris flow initiation. The hydraulic conductivity of the bed sediments is an important factor controlling the type and sequence of processes triggering debris flows. At lower K_s values, Hortonian overland will be the first process to start debris flows followed by bed failure or saturation overland flow. At higher K_s values, triggering by Hortonian overland flow is not possible anymore in this relatively coarse bed material, and triggering by bed failure will be the dominant process if the slope gradient is steep enough ($>16^\circ$). Therefore, the slope gradient of the channel bed is a second important factor controlling the type of hydro-mechanical triggering. On gentler slopes which remain stable under saturated conditions, saturation overland flow might create debris flows if slope gradient is not too gentle, and therefore sediment concentration too low to call it a debris flow.

We further analyzed also the effect of different important morphometric and hydro-mechanical parameters on meteorological thresholds for triggering debris flows by overland flow or bed failure, respectively. With respect to overland flow triggering, the morphometric factors related to the size of the source area and width and length of the channel bed have the largest influence on the position of the I-D curves. Meteorological thresholds for bed failure triggering are also sensitive to morphometric parameters while the hydro-mechanical parameters have relative less influence on these threshold values.

Author Contributions: T.W.J.v.A., B.Y. and W.H. conceived and designed the experiments; B.Y. performed the hydro-mechanical measurements on the materials and performed the experiments; T.W.J.v.A. and B.Y. analyzed the data; T.W.J.v.A. did the modelling and wrote the paper.

Funding: This research was funded by the National Natural Science Foundation of China (NSFC) grant number [41672341].

Acknowledgments: We thank the two anonymous reviewers and Niek Rengers for their valuable comments and suggestions which improved our paper.

Conflicts of Interest: The authors declare no conflict of interest.

References

1. Zhuang, J.; Cui, P.; Peng, J.; Hu, K.; Iqbal, J. Initiation process of debris flows on different slopes due to surface flow and trigger-specific strategies for mitigating post-earthquake in old Beichuan County, China. *Environ. Earth Sci.* **2013**, *68*, 1391–1403. [[CrossRef](#)]
2. Cuomo, S.; Della Sala, M. Rainfall-induced infiltration, runoff and failure in steep unsaturated shallow soil deposits. *Eng. Geol.* **2013**, *162*, 118–127. [[CrossRef](#)]
3. Cuomo, S.; Della Sala, M.; Novita, A. Physically based modelling of soil erosion induced by rainfall in small mountain basins. *Geomorphology* **2015**, *243*, 106–115. [[CrossRef](#)]
4. Berti, M.; Genevois, R.; Simoni, S.; Tecca, P.R. Field observations of a debris flow event in the Dolomites. *Geomorphology* **1999**, *29*, 265–274. [[CrossRef](#)]
5. Armanini, A.; Gregoretti, C. Triggering of debris flow by overland flow: A comparison between theoretical and experimental results. In Proceedings of the 2nd International Conference on Debris flow Hazards Mitigation, Taipei, Taiwan, 16–18 August 2000; pp. 117–124.
6. Takahashi, T. Initiation and flow of various types of debris flow. In Proceedings of the 2nd International Conference on Debris Flow Hazards Mitigation: Mechanics, Prediction and Assessment, Taipei, Taiwan, 16–18 August 2000; pp. 15–25.
7. Coe, J.A.; Kinner, D.A.; Godt, J.W. Initiation conditions for debris flows generated by runoff at Chalk Cliffs, central Colorado. *Geomorphology* **2008**, *96*, 270–297. [[CrossRef](#)]
8. Yu, B. Research on the prediction of debris flows triggered in channels. *Nat. Hazards* **2011**, *58*, 391–406. [[CrossRef](#)]
9. Van Asch, T.W.J.; Tang, C.; Zhu, J.; Alkema, D. An integrated model to assess critical rainfall thresholds for the critical run-out distances of debris flows. *Nat. Hazards* **2014**, *70*, 299–311. [[CrossRef](#)]

10. Tang, C.; Rengers, N.; Van Asch, T.W.J.; Yang, Y.H.; Wang, G.F. Triggering conditions and depositional characteristics of a disastrous debris-flow event in Zhouqu city, Gansu Province, northwestern China. *Nat. Hazards Earth Syst. Sci.* **2011**, *11*, 2903–2912. [[CrossRef](#)]
11. Cui, P.; Zhou, G.G.D.; Zhu, X.H.; Zhang, J.Q. Scale amplification of natural debris flows caused by cascading landslide dam failures. *Geomorphology* **2013**, *182*, 173–189. [[CrossRef](#)]
12. Zhou, G.G.D.; Cui, P.; Chen, H.Y.; Zhu, X.H.; Tang, J.B.; Sun, Q.C. Experimental study on cascading landslide dam failures by upstream flows. *Landslides* **2013**, *10*, 633–643. [[CrossRef](#)]
13. Hu, W.; Xu, Q.; van Asch, T.W.J.; Zhu, X.; Xu, Q.Q. Flume tests to study the initiation of huge debris flows after the Wenchuan earthquake in S-WChina. *Eng. Geol.* **2015**, *182*, 121–129. [[CrossRef](#)]
14. Cannon, S.H.; Kirkham, R.M.; Parise, M. Wildfire-related debris flow initiation processes, Storm King Mountain, Colorado. *Geomorphology* **2001**, *39*, 171–188. [[CrossRef](#)]
15. Hungr, O.; Evans, S.G.; Bovis, M.J.; Hutchinson, J.N. A review of the classification of landslides of the flow type. *Environ. Eng. Geosci.* **2001**, *7*, 221–238. [[CrossRef](#)]
16. Malet, J.-P.; Laigle, D.; Remaître, A.; Maquaire, O. Triggering conditions and mobility of debris flows associated to complex earthflows. *Geomorphology* **2005**, *66*, 215–235. [[CrossRef](#)]
17. Cascini, L.; Cuomo, S.; Della Sala, M. Spatial and temporal occurrence of rainfall induced shallow landslides of flow type: A case of Sarno-Quindici, Italy. *Geomorphology* **2011**, *126*, 148–158. [[CrossRef](#)]
18. Zhang, S.; Zhang, L.M.; Peng, M.; Zhang, L.L.; Zhao, H.F.; Chen, H.X. Assessment of risks of loose landslide deposits formed by the 2008 Wenchuan earthquake. *Nat. Hazards Earth Syst. Sci.* **2012**, *12*, 1381–1392. [[CrossRef](#)]
19. Iverson, R.M.; Reid, M.E.; LaHusen, R.G. Debris flow mobilization from landslides. *Ann. Rev. Earth Plan. Sci.* **1997**, *25*, 85–138. [[CrossRef](#)]
20. Fuchu, D.; Lee, C.F.; Sijing, W. Analysis of rainstorm-induced slide-debris flows on natural terrain of Lantau Island, Hong Kong. *Eng. Geol.* **1999**, *51*, 279–290. [[CrossRef](#)]
21. Gabet, E.J.; Mudd, S.M. The mobilization of debris flows from shallow landslides. *Geomorphology* **2006**, *74*, 207–218. [[CrossRef](#)]
22. Van Asch, T.W.J.; Malet, J.-P. Flow-type failures in fine-grained soils: An important aspect in landslide hazard analysis. *Nat. Hazards Earth Syst. Sci.* **2009**, *9*, 1703–1711. [[CrossRef](#)]
23. Hu, W.; Donga, X.J.; Xua, Q.; Wang, G.H.; Van Asch, T.W.J.; Hicher, P.Y. Initiation processes for overland flow generated debris flows in the Wenchuan earthquake area of China. *Geomorphology* **2016**, *253*, 468–477. [[CrossRef](#)]
24. Berti, M.; Simoni, A. Experimental evidences and numerical modelling of debris flow initiated by channel runoff. *Landslides* **2005**, *2*, 171–182. [[CrossRef](#)]
25. Kean, J.W.; McCoy, S.W.; Tucker, G.E.; Staley, D.M.; Coe, J.A. Runoff-generated debris flows: Observations and modeling of surge initiation, magnitude, and frequency. *J. Geophys. Res. Earth Surf.* **2013**, *118*, 2190–2207. [[CrossRef](#)]
26. Hu, W.; Xu, Q.; Wang, G.H.; van Asch, T.W.J.; Hicher, P.Y. Sensitivity of the initiation of debris flow to initial soil moisture. *Landslides* **2015**, *12*, 1139–1145. [[CrossRef](#)]
27. Liu, C.; Dong, J.; Peng, Y.; Huang, H. Effects of strong ground motion on the susceptibility of gully type debris flows. *Eng. Geol.* **2009**, *104*, 241–253. [[CrossRef](#)]
28. Chang, T.C.; Chien, Y.H. The application of genetic algorithm in debris flow prediction. *Environ. Geol.* **2007**, *53*, 339–347. [[CrossRef](#)]
29. Tiranti, D.; Bonetto, S.; Mandrone, G. Quantitative basin characterization to refine debris-flow triggering criteria and processes: An example from the Italian Western Alps. *Landslides* **2008**, *5*, 45–57. [[CrossRef](#)]
30. Yu, B.; Li, L.; Wu, Y.; Chu, S. A formation model for debris flows in the Chenyulan River Watershed, Taiwan. *Nat. Hazards* **2013**, *68*, 745–762. [[CrossRef](#)]
31. Smith, G.N.; Smith, I.G.N. *Elements of Soil Mechanics*, 7th ed.; Blackwell Science Ltd.: Oxford, UK, 1988; p. 494, ISBN 0-632-04126-9.
32. Hendriks, M.R. *Introduction to Physical Hydrology*, 1st ed.; Oxford University Press: Oxford, UK, 2010; p. 331, ISBN 978-0-19-929684-2.
33. Chow, V.T.; Maidment, D.R.; Mays, L.W. *Applied Hydrology*; McGraw-Hill Book Company: New York, NY, USA, 1988; p. 572, ISBN 0-07-010810-2.

34. Rickenmann, D. Hyperconcentrated flow and sediment transport at steep slopes. *J. Hydraul. Eng.* **1991**, *117*, 1419–1439. [[CrossRef](#)]
35. Rickenmann, D. Comparison of bed load transport in torrents and gravel bed streams. *Water Resour. Res.* **2001**, *37*, 3295–3305. [[CrossRef](#)]
36. United States Department of Agriculture (USDA-SCS). *National Engineering Handbook*; Section 4: Hydrology 1985; USDA-SCS: Washington, DC, USA, 1985.
37. Innes, J.L. Debris flows. *Prog. Phys. Geogr.* **1983**, *7*, 469–501. [[CrossRef](#)]
38. Chen, C.-Y.; Chen, T.-C.; Yu, F.-C.; Yu, W.-H.; Tseng, C.-C. Rainfall duration and debris-flow initiated studies for real-time monitoring. *Environ. Geol.* **2005**, *47*, 715–724. [[CrossRef](#)]
39. Caine, N. The rainfall intensity duration control of shallow landslides and debris flows. *Geogr. Ann. A Phys. Geogr.* **1980**, *62*, 23–27.
40. Stancanelli, L.; Lanzoni, M.S.; Foti, E. Propagation and deposition of stony debris flows at channel confluences. *Water Resour. Res.* **2015**, *51*, 5100–5116. [[CrossRef](#)]
41. George, D.L.; Iverson, R.M. A depth-averaged debris-flow model that includes the effects of evolving dilatancy I. Physical basis. *Proc. R. Soc.* **2014**, *A470*. [[CrossRef](#)]
42. Lehmann, P.; Or, D. Hydromechanical triggering of landslides: From progressive local failures to mass release. *Water Resour. Res.* **2012**, *48*, W03535. [[CrossRef](#)]
43. McDougall, S.; Hungr, O. Dynamic modelling of entrainment in rapid landslides. *Can. Geotech. J.* **2005**, *42*, 1437–1448. [[CrossRef](#)]
44. Medina, V.; Hürlimann, M.; Bateman, A. Application of FLATModel, a 2D finite volume code, to debris flows in the northeastern part of the Iberian Peninsula. *Landslides* **2008**, *5*, 127–142. [[CrossRef](#)]
45. Iverson, R.M.; Reid, M.E.; Logan, M.; LaHusen, R.G.; Godt, J.W.; Griswold, J.P. Positive feedback and momentum growth during debris-flow entrainment of wet bed sediment. *Nat. Geosci.* **2011**, *4*, 116–121. [[CrossRef](#)]
46. Quan Luna, B.; Remaître, A.; Van Asch, T.W.J.; Malet, J.-P.; Van Westen, C.J. Analysis of debris flow behavior with a one dimensional run-out model incorporating entrainment. *Eng. Geol.* **2012**, *128*, 63–75. [[CrossRef](#)]
47. Lanzoni, S.; Gregoretti, C.; Stancanelli, L.M. Coarse-grained debris flow dynamics on erodible beds. *J. Geophys. Res. Earth Surf.* **2017**, *122*. [[CrossRef](#)]



© 2018 by the authors. Licensee MDPI, Basel, Switzerland. This article is an open access article distributed under the terms and conditions of the Creative Commons Attribution (CC BY) license (<http://creativecommons.org/licenses/by/4.0/>).